

Accepted Manuscript

Title: High-Temperature Sensor Based on Peanut Flat-end Reflection Structure

Authors: Yina Li, Zixin Liang, Chunliu Zhao, Dongning Wang

PII: S0030-4026(17)30907-5
DOI: <http://dx.doi.org/doi:10.1016/j.ijleo.2017.08.015>
Reference: IJLEO 59478



To appear in:

Received date: 24-5-2017
Revised date: 17-7-2017
Accepted date: 2-8-2017

Please cite this article as: Yina Li, Zixin Liang, Chunliu Zhao, Dongning Wang, High-Temperature Sensor Based on Peanut Flat-end Reflection Structure, *Optik - International Journal for Light and Electron Optics* <http://dx.doi.org/10.1016/j.ijleo.2017.08.015>

This is a PDF file of an unedited manuscript that has been accepted for publication. As a service to our customers we are providing this early version of the manuscript. The manuscript will undergo copyediting, typesetting, and review of the resulting proof before it is published in its final form. Please note that during the production process errors may be discovered which could affect the content, and all legal disclaimers that apply to the journal pertain.

High-Temperature Sensor Based on Peanut Flat-end Reflection Structure

Yina Li, Zixin Liang, Chunliu Zhao*, Dongning Wang

Yina Li, Chunliu Zhao*, Dongning Wang are with the Institute of Optoelectronic Technology, China Jiliang University, Hangzhou, Zhejiang, 310018, China (e-mail: lia61994@126.com; zhchunliu@hotmail.com; dnwang@cjlu.edu.cn).

Zixin Liang is with the Australian National University, Acton, Canberra, ACT, 2601, Australia(e-mail: zoeliang413@gmail.com).

*Corresponding author : Chunliu Zhao (e-mail: zhchunliu@hotmail.com)

Abstract—A high-temperature sensor based on a peanut flat-end reflection structure is demonstrated. The sensor can be simply fabricated by splicing the spherical end-faces of two segments of single-mode fibers and then cleaving one other end as a flat reflect surface. The proposed structure works as a reflected interferometer. When the ambient temperature changes, the resonant dip wavelength of the interferometer will shift due to the linear expansion or contraction and the thermo-optic effect. As a result, the temperature measurement can be achieved by monitoring the resonant dip wavelength of the interferometer. Experimental results show that the proposed sensor probe based on the peanut flat-end reflection structure works well and it can measure the temperature range from 100 °C to 900 °C with the sensitivity of 0.098 nm/°C with $R^2=0.988$. When temperature ranges from 400°C to 900°C, the sensitivity of 0.11 nm/°C can be achieved with $R^2=0.9995$. Due to its compact and simple configuration, the proposed sensor is a good high temperature sensor probe.

Keywords—high-temperature, reflected interferometer , peanut flat-end

I. INTRODUCTION

Temperature, in scientific experiments and industrial productions, is one of the most important parameters which must be strictly controlled. So temperature measurements especially high temperature measurements are of great importance. Various types of optical fiber temperature sensors have been proposed. Among all the detecting methods, temperature sensors based on fiber Brag gratings (FBGs)[1-5] have attracted much attention due to their advantages on wavelength multiplexing for distributed measurements. However FBGs are usually fabricated by use of UV laser irradiation and the gratings fabricated in this way might not be operated at high temperature due to the tendency of being erased. In recent years, FBGs have been successfully fabricated by femtosecond laser pulse irradiation and exhibit excellent stability above 1000 °C [6-8]. However the cost of such femtosecond laser fabrication systems is high, limiting their widespread applications.

With the development of fiber technology, other interferometer-based temperature sensors have been proposed. Michelson-based high-temperature sensors are robust and cheap but sometimes they are needed to polish or twist[9-10] which means complex processes are required. Fabry-Perot based high-temperature sensors[11-13] are usually small and suitable for remote sensing, but some based on FPI have to make a extremely small air-gap cavity such as positioning a glass microsphere in a capillary tube[12]which is a

complex fabrication process. For example, the Fabry-Perot interferometer (FPI) based on a solid-core PCF can reach a sensitivity of $13.8 \text{ pm}/^\circ\text{C}$ as the temperature increases to $600 \text{ }^\circ\text{C}$ [14], which special fibers are needed. The temperature sensor based on core diameter mismatch can measure temperature stably up to more than $900 \text{ }^\circ\text{C}$ with the sensitivity of $0.088 \text{ nm}/^\circ\text{C}$ [15], however, the sensing area are too long. These sensors mentioned above exist advantages and some disadvantages. Some are unsuitable for long-distance sensing because they work on transmission [14]. Some need femtosecond laser pulse irradiation which are expensive [16-17].

In this paper, we propose a high-temperature sensor based on a peanut flat-end reflection structure. This sensor is fabricated by making a peanut-shape structure through splicing the spherical end-faces of two segments of single-mode fibers (SMFs) and then cleaving one other end as a flat reflect surface. The proposed structure works as a reflected interferometer so that it is suitable for long-distance detecting the variation of temperature at the proposed sensor head. The temperature measurement can be achieved by monitoring the resonant dip wavelength of the interferometer. Due to its compact and simple configuration, the proposed sensor provides a feasible and cheap structure to achieve wide range and high sensitivity detection of the high temperature.

II. EXPERIMENTAL SETUP AND SENSOR PRINCIPLE

A. Experimental Setup

Fig.1 shows the experimental setup of a high-temperature measurement with a peanut flat-end reflection structure. Light from a broadband light source (BBS) transmits to a 3-dB fiber coupler through a SMF. The fiber coupler is used to transmit light to the peanut flat-end reflection structure. And the reflected light of the proposed structure is transmitted back to an optical spectrum analyzer (OSA, YOKOGAWA) through the fiber coupler. The wavelength range of the BBS covers from 1400 nm to 1600 nm and the resolution of OSA is 0.05 nm . In the experiments, the temperature of electrical resistance furnace (Shanghai Y-FENG, SX2-4-10, rated power: 4 kw) is increased from room temperature to $900 \text{ }^\circ\text{C}$, each time $100 \text{ }^\circ\text{C}$, and is maintained for ~ 3 minutes. The melt temperature of silica is around $1600 \text{ }^\circ\text{C}$, because of the limitation of the maximum temperature of electrical resistance furnace, the temperature range of experiment is under 900°C .

Fig.2 shows the optical microscopic image of the peanut flat-end reflection structure. The proposed structure is composed of two spherical end-faces. These two spherical end-faces form a peanut shape structure. The diameters of two spherical end-faces are $100.6 \text{ }\mu\text{m}$ and $100.6 \text{ }\mu\text{m}$, respectively. The length of the peanut structure is $385.4 \text{ }\mu\text{m}$, the splice of two spheres is $92.4 \text{ }\mu\text{m}$ and the distance between the reflect surface and the peanut-shape (d in Fig.3) is 2 cm .

In the fabrication processes, by using a commercial fiber fusion splicer (FSM-62S), the proper electrical arc discharges are applied on the flat end-face of a SMF [18], then the flat end-face become a spherical end-face. Another spherical end-face of the SMF is made in the same way. The diameter of spherical end-face depends on the number of discharge. The more discharge times, the larger the diameter. During the fabrication process, seven times of discharge are applied to the flat end-face. The discharge time is 3000 ms . Then, the peanut-shape structure is made by splicing two spherical end-faces of SMFs. An optical fiber cleaver is used to make a flat end-face at the right end of the peanut-shape structure. This flat end-face (the purple surface marked in Fig.3) works as a reflect surface.

B. Sensor Principle

The schematic diagram of the peanut flat-end reflection sensor probe is shown in Fig.3. The sphere can diverge the light when an optical signal transmits into it. Hence, when light (the black arrows marked in Fig.3) transmits into the first sphere of the peanut-shape structure, there will be a little energy of the core mode coupled into the cladding. Therefore the input optical signal is split into two paths, the core and the cladding. In order to make more energy couple into the cladding, two spheres are cascaded and they form a peanut-shape structure. When the optical signals transmit to the second sphere, more energy will couple into the

cladding. This two optical signals, transmitting in the core and the cladding, are both reflected by the flat end-face (the purple surface marked in Fig.3). This two reflected optical signals (the red arrows marked in Fig.3) go back as the same way. They are recombined together at the left segment of the SMF and the interference happens. An optical path difference Δ is produced by two signals transmitting in the core and in the cladding which is given by

$$\Delta = \Delta n_{eff} \cdot 2L \quad (1)$$

where Δn_{eff} is the effective refractive index difference between the core mode and the cladding mode, L is the interaction length. Because the proposed sensor is based on the reflected interference, the interference length is twice the length of L . The optical phase difference $\Delta\Phi$ is given by

$$\Delta\Phi = 2\pi\Delta / \lambda = 4\pi\Delta n_{eff} L / \lambda \quad (2)$$

$$\Delta n_{eff} = n_{eff}^{co} - n_{eff}^{cl} \quad (3)$$

where λ is the input wavelength. n_{eff}^{co} and n_{eff}^{cl} are the effective refractive index of the core mode and the cladding mode, respectively.

When $\Delta\Phi$ equals to $(2m+1)\pi$, $m=1,2,3,\dots$, λ in the equation 2 is the dip value of the interference waves, the dip wavelength satisfies the equation of [19]:

$$\lambda = 4\Delta n_{eff} L / (2m+1) \quad (4)$$

The proposed sensors with different lengths of d , 1cm and 2cm are fabricated and the interference spectra at room temperature are shown in Fig.4. The fringes visibilities of over ~ 10 dB and ~ 5 dB and the dips number of 5 and 2, respectively, are obtained in the wavelength region of 1530nm to 1560nm. According to the equation 1, the optical path difference depends on the length of L . During the fabricate processes, the length of the peanut-shape almost stays the same. It is the changes of d result in the differences of L . Hence, as shown in Fig.4, the longer the d is, the denser the interference dips become. The contrast of fringes would be improved by a longer length of d .

When the ambient temperature changes, the resonant dip wavelength will shift by linear expansion or contraction and the thermo-optic effect. The interaction length will increase because of linear expansion caused by temperature increasing and at the same time the effective refractive index may also be changed due to the thermo-optic effect of the fiber [20]. Thus, by differentiating the equation 4, the temperature sensitivity can be written as:

$$\begin{aligned} \frac{\Delta\lambda}{\Delta T} &= \frac{4}{2m+1} \left(\frac{\partial \Delta n_{eff}}{\partial T} L_0 + \frac{\partial L}{\partial T} \Delta n_{eff}^0 \right) \quad (5) \\ &= \frac{4}{2m+1} \left(\frac{\partial (n_{eff}^{co} - n_{eff}^{cl})}{\partial T} L_0 + \frac{\partial L}{\partial T} \Delta n_{eff}^0 \right) \end{aligned}$$

here L_0 is the length of interaction length at initial temperature, Δn_{eff}^0 is the effective RI difference between the core mode and the cladding mode at initial temperature. According to the equation 4, it is the variations of Δn_{eff} and L that cause the differences of the dip wavelength, and based on the equation 5, we have:

$$\Delta\lambda / \Delta T = \frac{1}{2m+1} [(k_{co} - k_{cl}) + \xi] \quad (6)$$

where k_{co} , k_{cl} are the thermo-optic coefficient of the core and the cladding, respectively, and ξ is the linear expansion coefficient of fiber. The thermo-optic coefficient is $\sim 10^{-6}$ and the linear expansion coefficient of fiber is $\sim 0.55 \times 10^{-6} \text{ } ^\circ\text{C}^{-1}$, they are all constants [10]. So the resonant wavelength increases linearly as temperature increases.

III. EXPERIMENTAL RESULTS AND DISCUSSION

During the course of applying temperature, the effect of the fiber coating burned might give undesirable strain on sensing head[15]. Hence the proposed sensor was heated to 800 °C and maintained there for 2 hours. This process called pretreatment. The burnt fiber coating induced effects will be removed, so that whether the dopant diffusion could seriously deteriorate the interference spectrum will be examined[21]. Fig.5 shows the interference spectrum of the peanut flat-end reflection structure after pretreatment.

As shown in Fig.5, six resonant dips of the proposed sensor probe can be observed in the wavelength range from 1490 nm to 1560 nm. The curve of the interference spectrum can be seen as a periodic curve and the free spectrum range is ~13 nm .

Fig.6(a) shows the interference spectra of the peanut flat-end reflection structure in response to temperature that changes from room temperature to 900 °C. Part of interference spectra which temperature range is from room temperature to 200 °C are shown in Fig.6(b) for better understanding. Dips of the interference spectra are very sharp so that they are easy to distinguish and analyze. Due to the linear expansion and the thermo-optic effect, the spectra shift about 10 nm/100 °C towards longer wavelength as temperature increasing. The interference fringes are somehow inhomogeneous since the core mode interferes with more than two cladding modes.

In order to observe the wavelength shift, one dip at the wavelength about 1515nm is chosen during our experiments. Fig.7 shows the relationships between dip wavelength and temperature in different temperature ranges. The relationships in two temperature ranges are analyzed in order to evaluate the performance of the proposed sensor in high temperature responses. From 100 °C to 900 °C, as shown in Fig.7(a), the fitting function is $y=0.098x+1500.6$ (function (a)) and the linear correlation coefficient is 0.988. From 400 °C to 900 °C, as shown in Fig.7(b), the fitting function is $y=0.11x+1491.87$ (function (b)) and the linear correlation coefficient is 0.9995. It is noted that the linear correlation coefficient of Fig.7(b) is 0.9995, which is higher than 0.988 of Fig.7(a). So when temperature ranges from 400 °C to 900 °C, the sensor probe has better linearity in temperature responses. Table I is the comparison between the true temperature and the measured temperature calculated by different fitting functions shown in Fig.7(a) and (b), respectively. Compared to true temperature, there are certain differences ~10 °C calculated by function (a) and no more than 3.8 °C calculated by function (b). Apparently, the proposed sensor probe has better linearity in high temperature responses.

In order to evaluate the performance of the proposed sensor, we repeat the temperature measurements three times. Since a natural temperature decreasing process from 900 °C to room temperature need about 12 hours, so temperature measurement ranges are reduced. The first heating period is from room temperature to 900 °C, the second heating period is from 400 °C to 900 °C, and the third heating period is from 450 °C to 900 °C. Fig.8 shows the relationships between the measured dip wavelength and temperature in three heating periods. As shown in Fig.8, the relationships between dip wavelength and temperature are linear, and all dip wavelengths show a good consistency in three heating cycles. By comparing the data of three times temperature measurements, the maximum error of three heating period is ~0.6 °C at 500 °C. The few discrepancies can be explained by the error of electrical resistance furnace. Because the natural temperature decreasing process is slow, there is a difference between the display temperature and the actual temperature. Additionally, when temperature ranges from 400 °C to 900 °C, the proposed sensor has better linearity and repeatability in temperature responses, which means that this sensor is suitable for high temperature monitoring.

Table II is the summary of characteristics of optical fiber high-temperature sensors based on various structures. Table II tells that high-temperature sensors that generally reported can achieve a sensitivity about

tens pm/°C, for example, 13.32 pm/°C of the temperature sensor based on 45 angled reflector [10], and 14.72pm/°C of the temperature sensor based on Michelson inline interferometer[16]. Compared with those previously interferometer-based temperature sensors, the proposed sensor probe shows advantages of cheap, easy fabrication, wide measurement range, and high temperature sensitivity. The peanut flat-end reflection structure is made by SMFs which is cheap. The interference spectra dips of this sensor probe are sharp so that it is easier to distinguish the dip wavelength. Additionally, this sensor probe has good linearity, repeatability and is suitable for long-distance detecting the variation of temperature at the proposed sensor head because it works on reflection.

IV. CONCLUSION

In summary, we propose a high-temperature sensor probe based on a peanut flat-end reflection structure. In the fabrication processes, by using a commercial fiber fusion splicer, the flat end-face of a SMF become a spherical end-face. The peanut-shape structure is made by splicing the spherical end-faces of two segments of SMFs. Then cleaving one other end as a flat reflect surface. When the ambient temperature changes, the resonant dip wavelength will shift by linear expansion or contraction and the thermo-optic effect. The resonant wavelength increases linearly as temperature increases. So that the temperature measurement can be achieved by monitoring the resonant dip wavelength of the interferometer. Experimental results show that the proposed sensor probe based on the peanut flat-end reflection structure works well and it can measure temperature range from room temperature to 900 °C with the sensitivity of 0.098 nm/°C. When temperature ranges from 400°C to 900°C, the sensitivity of 0.11 nm/°C can be achieved with $R^2=0.9995$. The proposed sensor probe can achieve higher sensitivity when in high-temperature range and has better linearity in temperature responses at the same time. Due to its compact and simple configuration, it provides a feasible and cheap structure to achieve wide range and high sensitivity detection of the high temperature.

Acknowledgments

This work is supported by the Natural Science Foundation of Zhejiang Province China under Grant No.LY17F050010.

REFERENCES:

- [1] J. Jung, H. Nam, B. Lee, J. O. Byun, and N. S. Kim, "Fiber Bragg grating temperature sensor with controllable sensitivity.," *Applied Optics*, vol. 38, pp. 2752-2754, 1999.
- [2] W. Zhou, C. Zhao, J. Huang, and X. Dong, "A Novel FBG Sensing Head Geometry for Strain-Temperature Discrimination," *Proceedings of SPIE - The International Society for Optical Engineering*, vol. 7634, pp. 1-6, 2009.
- [3] S. Gupta, "Low Temperature Sensing Using Fiber Bragg Gratings," *Optical Fiber Sensors*, 1996.
- [4] A. Siekiera, R. Engelbrecht, L. Bueth, and B. Schmauss, "Simultaneous Sensing of Temperature and Strain by Combined FBG and Mode-Interference Sensors," *Bragg Gratings, Photosensitivity, & Poling in G...*, 2012.
- [5] T. Osuch, K. Markowski, A. Manujło, and K. Jędrzejewski, "Coupling independent fiber optic tilt and temperature sensor based on chirped tapered fiber Bragg grating in double-pass configuration," *Sensors and Actuators A: Physical*, 2016.
- [6] Y. Li, C. R. Liao, D. N. Wang, T. Sun, and K. T. V. Grattan, "Study of spectral and annealing properties of fiber Bragg gratings written in H₂-free and H₂- loaded fibers by use of femtosecond laser pulses," *Optics express*, vol. 16, p. 21239, 2008.
- [7] C. Smelser, S. Mihailov and D. Grobnc, "Formation of Type I-IR and Type II-IR gratings with an ultrafast IR laser and a phase mask.," *Optics Express*, 2005.

- [8] C. Liao, D. N. Wang, Y. Li, T. Sun, and K. T. Grattan, "Temporal thermal response of Type II-IR fiber Bragg gratings," *Applied Optics*, 2009.
- [9] Zhao N, Fu H, Shao M, et al. High temperature probe sensor with high sensitivity based on Michelson interferometer[J]. *Optics Communications*, 2013, 343(8):131-134.
- [10] Yin J, Liu T, Jiang J, et al. Assembly-Free-Based Fiber-Optic Micro-Michelson Interferometer for High Temperature Sensing[J]. *IEEE Photonics Technology Letters*, 2016, 28(6):625-628.
- [11] T. Wei, Y. Han, H. L. Tsai, and H. Xiao, "Miniaturized fiber inline Fabry-Perot interferometer fabricated with a femtosecond laser," *Opt Lett*, vol. 33, pp. 536-8, 2008-03-15 2008.
- [12] B. Xu, Y. M. Liu, D. N. Wang, and J. Q. Li, "Fiber Fabry-Pérot Interferometer for Measurement of Gas Pressure and Temperature," *Journal of Lightwave Technology*, vol. 34, pp. 4920-4925, 2016.
- [13] T. Liu, J. Yin, J. Jiang, K. Liu, S. Wang, and S. Zou, "Differential-pressure-based fiber-optic temperature sensor using Fabry-Perot interferometry," *OPTICS LETTERS*, vol. 40, pp. 1049-1052, 2015.
- [14] J. Zhang, H. Sun, Q. Rong, Y. Ma, L. Liang, Q. Xu, P. Zhao, Z. Feng, M. Hu, and X. Qiao, "High-temperature sensor using a Fabry-Perot interferometer based on solid-core photonic crystal fiber," *CHINESE OPTICS LETTERS*, vol. 10, pp. 27-29, 2012-07-10 2012.
- [15] L. V. Nguyen, D. Hwang, S. Moon, D. S. Moon, and Y. Chung, "High temperature fiber sensor with high sensitivity based on core diameter mismatch.," *Optics Express*, 2008.
- [16] L. Yuan, T. Wei, Q. Han, H. Wang, J. Huang, L. Jiang, and H. Xiao, "Fiber inline Michelson interferometer fabricated by a femtosecond laser," *OPTICS LETTERS*, vol. 37, pp. 4489-4491, 2012.
- [17] Y. Liu, S. Qu and Y. Li, "Single microchannel high-temperature fiber sensor by femtosecond laser-induced water breakdown," *OPTICS LETTERS*, vol. 38, pp. 335-337, 2013.
- [18] D. Wu, T. Zhu, K. S. Chiang, and M. Deng, "All Single-Mode Fiber Mach-Zehnder Interferometer Based on Two Peanut-Shape Structures," *Journal of Lightwave Technology*, vol. 30, pp. 805-810, 2012.
- [19] H. Gong, X. Yang, K. Ni, C. Zhao, and X. Dong, "An Optical Fiber Curvature Sensor Based on Two Peanut-Shape Structures Modal Interferometer," *IEEE Photonics Technology Letters*, vol. 26, pp. 22-24, 2014.
- [20] C. L. Zhao, L. Xiao, J. Ju, M. S. Demokan, and W. Jin, "Strain and Temperature Characteristics of a Long-Period Grating Written in a Photonic Crystal Fiber and Its Application as a Temperature-Insensitive Strain Sensor," *Journal of Lightwave Technology*, vol. 26, pp. 220-227, 2008.
- [21] Y. Wang, Y. Li, C. Liao, D. N. Wang, M. Yang, and P. Lu, "High-Temperature Sensing Using Miniaturized Fiber In-Line Mach-Zehnder Interferometer," *IEEE Photonics Technology Letters*, vol. 22, pp. 39-41, 2010.
- [22] L. Xiong, D. Zhang, L. Li, and Y. Guo, "EFPI-FBG hybrid sensor for simultaneous measurement of high temperature and large strain (Chinese Title: EFPI-FBG hybrid sensor for simultaneous measurement of high temperature and large strain)," *Chinese Optics Letters*, vol. 12, pp. 29-33, 2014.

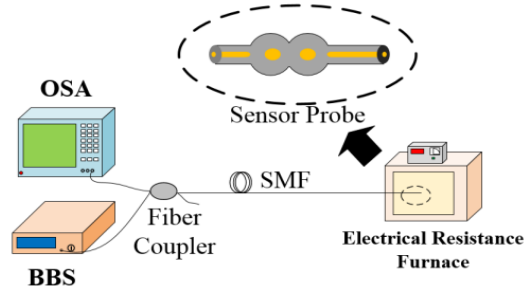


Fig.1. System configuration for experimental setup of high-temperature measurement with peanut flat-end reflection structure.

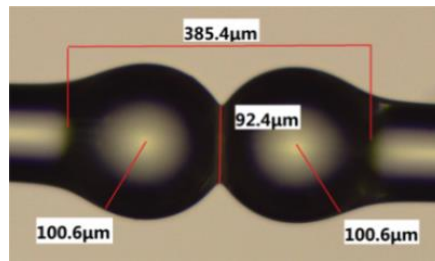


Fig.2. Optical microscopic image of the peanut flat-end reflection structure.

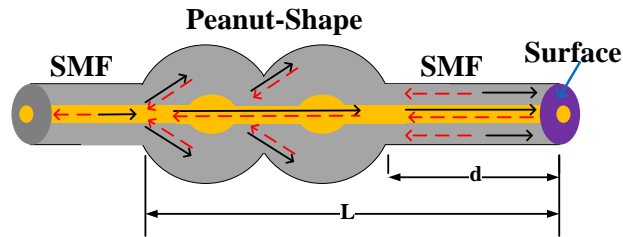


Fig.3. Schematic diagram of the peanut flat-end reflection sensor probe.

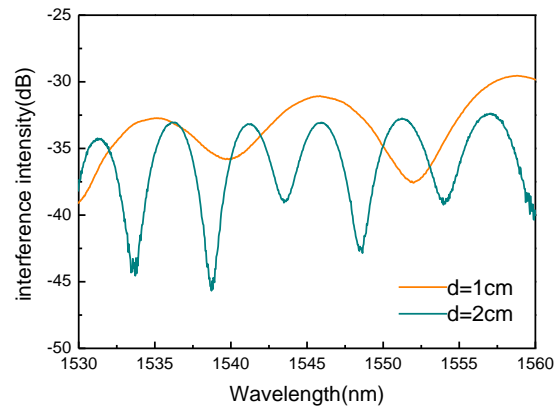


Fig.4. Interference spectra of the proposed sensors with $d=1\text{cm}$ and $d=2\text{cm}$, respectively, at room temperature.

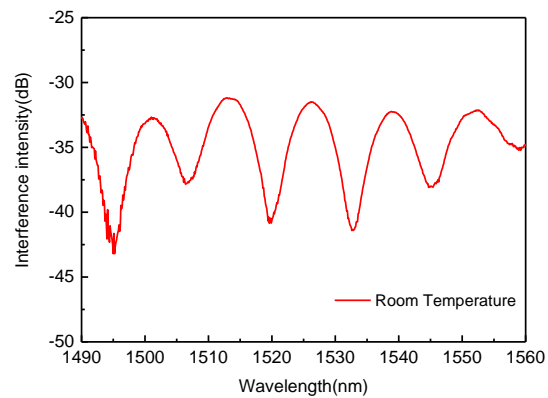


Fig.5. The interference spectrum of peanut flat-end reflection structure after pretreatment that heated to 800°C then maintained for 2 hours.

(b)

(a)

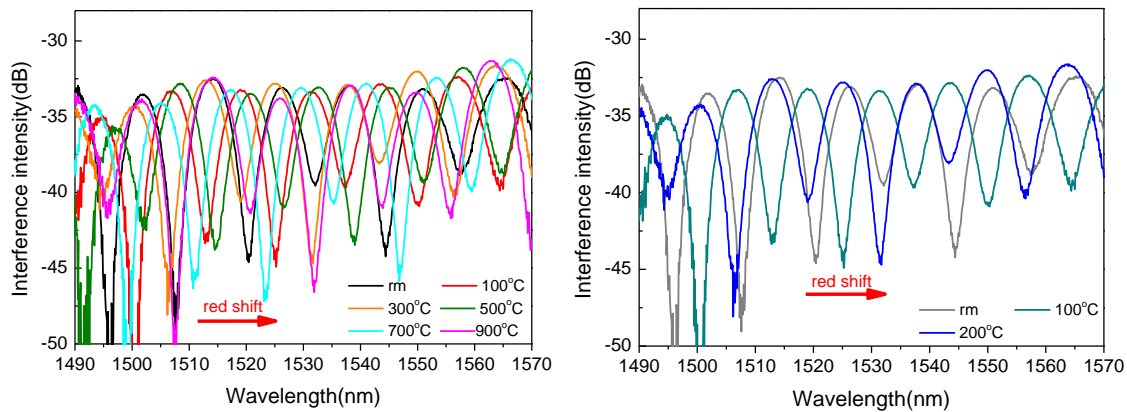


Fig.6. Interference spectra of peanut flat-end reflection structure in response to temperature changes. (a) temperature ranges from room temperature to 900°C. (b) temperature ranges from room temperature to 200°C.

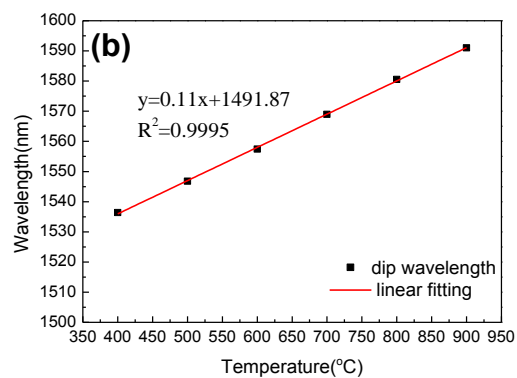
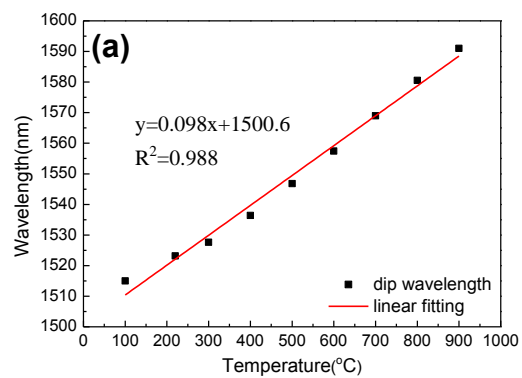


Fig.7. The relationships between dip wavelength and temperature. (a) temperature ranges from 100 °C to 900 °C and (b) temperature ranges from 400 °C to 900 °C.

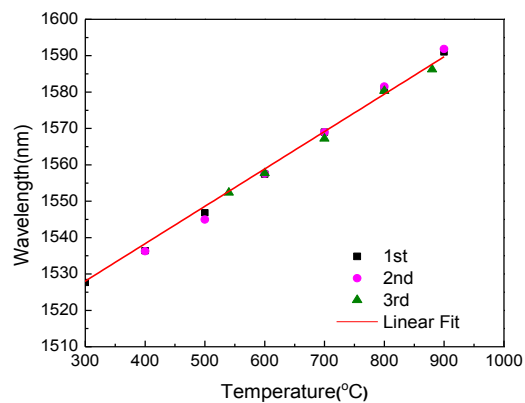


Fig.8.The relationships between the measured dip wavelength and temperature in three heating periods.

TABLE I

Comparison between the true temperature and the measured temperature calculated by different fitting functions shown in Fig.7(a) and (b) respectively

True Temperature (°C)	Measured Temperature (°C)	
	Calculated by function (a)	Calculated by function (b)
400	389.8	403.2
500	480.7	501.3
600	591.1	599.5
700	701.3	700.8
800	811.1	803.8
900	915.3	902.8

TABLE II

Sensor	Sensitivity	Measurement range
Based on ultracompact FPI[14]	13.8 pm/°C	33°C~ 600 °C
Based on core diameter mismatch[15]	88 pm/°C	30°C~900 °C
Based on 45 angled reflector[10]	13.32pm/°C	19°C~ 950 °C
Based on EFPI-FBG[22]	13.6 pm/°C	Up to 500 °C
Proposed sensor	0.11nm/°C	Up to 900 °C

Summary of characteristics of optical fiber high-temperature sensors based on various structures